CEAS-GNC-2022-064

CEAS EuroGNC 2022
"Conference on Guidance, Navigation and Control"
3-5 May 2022 @ Technische Universität Berlin, Germany

A Novel Adaptive Aeroservoelastic Coupling Suppression Algorithm for the A330 SMART MRTT Flying Boom Control Laws

Rodney Rodríguez Robles Lead Guidance, Navigation and Control Engineer, Airbus UpNext, Autonomy Demonstrator, 28906, Getafe, Spain. rodney.rodriguez@airbus.com

The A330 SMART MRTT program will develop, certify and implement Automatic Air-to-Air Refuelling (A3R) capability as well as enhanced and more resilient adaptive Flying Boom Control Laws, among other functionalities. The present paper describes a novel algorithm developed to provide robust and adaptive aeroservoelastic coupling suppression functionalities to the Flying Boom Control Laws, by means of the cancelation of the elastic modes component in the attitudes and angular rates feedback signals, while maintaining the components related to the rigid dynamics of the system unaltered. The algorithm uses an adaptive elastic mode identification technique in combination with an exogenous boundary physical condition estimator to optimally fuse the measured signals, providing excellent aeroservoelastic coupling suppression performances for every phase of the refuelling operation. Results obtained during the development flight test campaign performed with both the A310 MRTT testbed and the A330 SMART MRTT platforms will be presented to validate the robustness and performance of the proposed algorithm.

Keywords: Aeroservoelastic Coupling Suppression; Adaptive Control; Very Flexible Structures

Nomenclature

N	=	Number of elastic modes
y_n^X	=	n^{th} sample of a discrete signal provided by a measurement source X
v_n^X	=	Measurement noise of a generic measurement source X
l_X	=	Spatial location of sensors X
Y_n^{FA}	=	Filtered signal in Free-Air condition
Y_n^C	=	Filtered signal in Coupled condition
Y_n^{EMAC}	=	EMAC filtered signal output
P_n	=	Probability of the ARBS being in a restricted movement status
K_n^i	=	Elastic mode cancellation parameters of the i^{th} elastic mode
r_n	=	Rigid dynamics
γ_n^i	=	Elastic activity of the i^{th} elastic mode
ω_n^i	=	Augmented frequency of the i^{th} elastic mode
$\varphi_n^i(l_X)$	=	Unitary displacements of the elastic mode i at sensor location l_X
L_n	=	Measured telescopic beam length
M_n	=	Measured Mach number
σ	=	Small approximation error

W_{jk}^{i} = Weight ij of the ANN of the i^{th} elastic mode

ϕ_{jk}^{i} = Activation functions of the ANN of the i^{th} elastic mode

λ_{jk_n} = Learning gain

E_n^i = Cancellation error

G_i = Static learning gain of the estimation kernel of the i^{th} elastic mode

ϵ_i = Threshold of the dead-band for the i^{th} elastic mode

φ = Unknown phase angle

ζ_n^i = Notch-filter output

J_n^i = Frequency cost function for the i^{th} elastic mode

$\boldsymbol{\Xi}$ = Matrix containing all elastic modes unitary displacement at sensors locations

$\boldsymbol{\theta}_n$ = Time-varying vector containing the weight coefficients of the spatial filter

$\hat{\beta}_n^s$ = Virtual signal

$\xi_n^{i,s}$ = Parameter that are modified online to grant that the virtual signals are linearly independent with respect to their elastic modes content

Δt = Discrete sample time

ANN = Artificial Neural Network

ARBS = Aerial Refuelling Boom System

ASECS = Aeroservoelastic Coupling Suppression

BCLAWs = Boom Flight Control Laws

CMM = Control Mode Mismatch

EMAC = Elastic Modes Adaptive Cancellation

FNN = Fuzzy Neural Network

MRTT = Multi-Role Transport Tanker

RIBS = Rigid Body Synthetic Sensor

1 Introduction

Throughout aerospace history, many incidents have emphasized the significant role that aeroservoelasticity plays in the dynamics of highly augmented aircraft with flexible structures [1, 2]. The stability of these types of systems is determined by the interaction between the aircraft's non-stationary aerodynamic forces, the flexible structure dynamics, and the flight control system dynamics. Without a proper Aeroservoelastic Coupling Suppression (ASECS) functionality in the flight control system, instabilities and handling qualities degradations could appear well below the flutter speed. From an energy-balance point of view, the onset of aeroservoelastic coupling instability is triggered when the flight control system and the non-stationary aerodynamic forces inject more energy into the system than the flexible structure can dissipate.

The main objective of ASECS methodologies is to render unobservable the displacements of the flexible structure to the controller, breaking any coupling between the control effectors' commands and the elastic dynamics of the flexible structure. Currently, notch-filtering is one of the most widely used ASECS methodologies in the aerospace industry [3], as it is the best and simplest solution for aircraft where the elastic modes' frequencies lie outside the control frequency bandwidth of the rigid plant. In the particular case of highly augmented aircraft with very flexible structures, the notch-filtering methodology is no longer suitable to remove the elastic modes' component from the feedback signals, given the large

phase lag and attenuation it introduces in the low-frequency bandwidth. Then, for aircraft or systems with very flexible structures, it is essential to apply alternative ASECS methodologies.

Alternative solutions, like extended Kalman filters observers [4] and modal filters [5] have been also investigated to provide an estimated elastic activity of very flexible structures, with potential use in ASECS problems. Alternatively, recent developments have tackled the ASECS problem from an optimal control perspective, via the minimization of the flexible state's observability and the maximization of the elastic modes controllability [6]. In addition to these solutions, the Rigid Body Synthetic Sensor (RIBS) approach [7] investigated for the B-2 Spirit has proved also to be a well-performing methodology for ASECS applications when a spatial sensor array is available and the elastic modes' shapes are perfectly known beforehand. Similar spatial filtering solutions have been investigated in [8].

Nevertheless, all of the previous solutions, like all model-based deterministic ASECS methodologies, present several major drawbacks that prevent their direct application to the Aerial Refueling Boom System (ARBS) installed in the A330 Multi-Role Transport Tanker (MRTT), a flexible slender structure with highly non-linear aerodynamics and fast-time-varying aeroelastic characteristics that strongly depend on the flight condition, the telescopic beam length, and the exogenous physical boundary conditions acting on the nozzle tip. One of the main drawbacks of Kalman and modal filtering techniques is their lack of robustness and adaptation capabilities against time-varying aeroservoelastic uncertainties that can depend even on the receiver aircraft's aerodynamics. Additionally, these methodologies, including RIBS, cannot cope with undetected changes in the exogenous physical boundary conditions acting on the ARBS's nozzle (altering the characteristics of the aeroelastic mode). Furthermore, spatial-filter methodologies like RIBS, would require expensive retrofits and modifications of the hardware and sensors of the ARBS to generate a spatial array of sensors.

To tackle these deficiencies, Airbus Defence and Space initiated a special Research and Technology (R&T) project for the new A330 SMART MRTT program. The objective of this project was to fast-develop novel adaptive ASECS methodologies that could further improve the BCLAWs performance and increase their robustness to aeroservoelastic coupling phenomena using only two measurement sources to cancel a generic number of elastic modes, as opposed to other adaptive algorithms [9]. The outcome of this R&T project was the Elastic Modes Adaptive Cancellation (EMAC), a novel ASECS methodology that delivers two unique functionalities to the BCLAWs, first, it provides adaptive multi-modal aeroservoelastic coupling suppression capabilities via an adaptive feedback mixing strategy requiring only two sensors already available in the ARBS; and second, it provides an estimated probability for the ARBS to be in physically Free-Air or in Coupled conditions (in contact with the receiver aircraft) based on the estimated elastic activity. These functionalities interlace to provide unmatched ASECS capabilities independently of undetected discrete changes of the exogenous physical boundary conditions of the ARBS.

These features provide the new BCLAWs with unparalleled robustness to undetected operational failures that might derive into a Control Mode Mismatch (CMM) condition, an abnormal aeroservoelastic-coupling-prone condition that occurs when there is an incoherence between the BCLAWs control mode being active and the exogenous physical boundary condition acting on the ARBS' nozzle (e.g. CLAWs being in "free-air" control mode, but the ARBS being actually latched within the receivers' receptacle). Moreover, the adaptability of the EMAC algorithm also offers improved robustness against variations of the aeroelastic properties of an aging structure, which will protect the ARBS from any potential handling qualities degradation at the end of its operational life.

The present paper aims to provide a high-level description of the EMAC algorithm's architecture, subsystems, and all their functionalities, including a formal description of their mathematical formulation, and finally, to present the flight test campaign results with the A310 MRTT Flight Testbed and the A330 SMART MRTT.

2 The Elastic Modes Adaptive Cancellation Algorithm

The Elastic Modes Adaptive Cancellation (EMAC) algorithm can be defined as an adaptive spatial filtering algorithm that requires only two input signals provided by two dissimilar sensors to suppress N elastic modes, while maintaining the rigid dynamics in the output signal unaltered. In the specific case of the ARBS, these two measurement sources are: a potentiometer located at the ARBS' ball joint, denoted by A, that measures angular displacements; and an IMU, denoted by B, located at the bulb close to the ruddervators' hinge, which provides angular rates and accelerations. Using the rigid-body kinematic equations, angular rates measurements provided by sensor B can be converted to angular displacements (attitudes), and vice versa. Both sensors A and B have been depicted in Fig. 1 along with the high-level architecture of the EMAC algorithm.

In the EMAC algorithm, measurements from sensors A and B are first pre-conditioned for dissimilar-sensor lag synchronization. Then, these conditioned signals are fed to a collection of $N_{FA} + N_C$ adaptive estimation kernels (N_{FA} elastic modes in Free-Air conditions and N_C elastic modes in Coupled conditions) that first identify the elastic modes' shapes and augmented frequencies via adaptive Artificial Neural Networks (ANN), and second, they provide the estimated activity of each selected elastic mode.

The information of the elastic modes' characteristics (shape and augmented frequency) and the estimated elastic activities are feedforwarded to two different modules that run in parallel, called the elastic modes cancellation modules. One module is dedicated to cancel N_{FA} elastic modes assuming the ARBS is in free-air conditions, and its counterpart module is dedicated to cancel N_C elastic modes assuming the ARBS is in restricted-movement conditions (latched or in contact with the receiver aircraft). These modules use an adaptive virtual sensor generation algorithm developed to overcome the limitations of the standard spatial filtering technique used in the RIBS methodology, to be able to cancel N elastic modes without requiring a spatial array of $N + 1$ sensors. This algorithm artificially generates $N - 1$ virtual sensors via a linear combination of the signals y_n^A and y_n^B, provided by sensor A and B respectively, and the estimated modal activities, in such a way that both the non-virtual signals y_n^A and y_n^B, and the virtual signals are linearly independent with respect to their modal activity.

In a posterior step, the set of $N - 1$ virtual signals is feedforwarded to an algebraic solver subsystem within each elastic modes cancellation module, where a standard spatial filtering technique is applied. This spatial filter combines the signals y_n^A and y_n^B, and the $N - 1$ virtual signals to cancel the components of the N elastic modes while maintaining unaltered the rigid dynamics of the ARBS in the output signal.

In parallel with the elastic modes cancellation modules, another estimator computes the probability of the ARBS being in a restricted movement status, denoted by P_n, using the estimated relative activity of the free-air and restricted movement elastic modes, and the current BCLAWs control mode being active (FREE AIR, COUPLED or DISCON FLIGHT).

Finally, the probability P_n is then feedforwarded to a signal-fader module that computes the weighted-probability sum of the filtered signals Y_n^{FA} and Y_n^C generated by the elastic modes cancellation

modules. The output of this module, denoted by Y_n^{EMAC}, is the filtered feedback signal that will be used by the BCLAWs' inner and outer loop controllers.

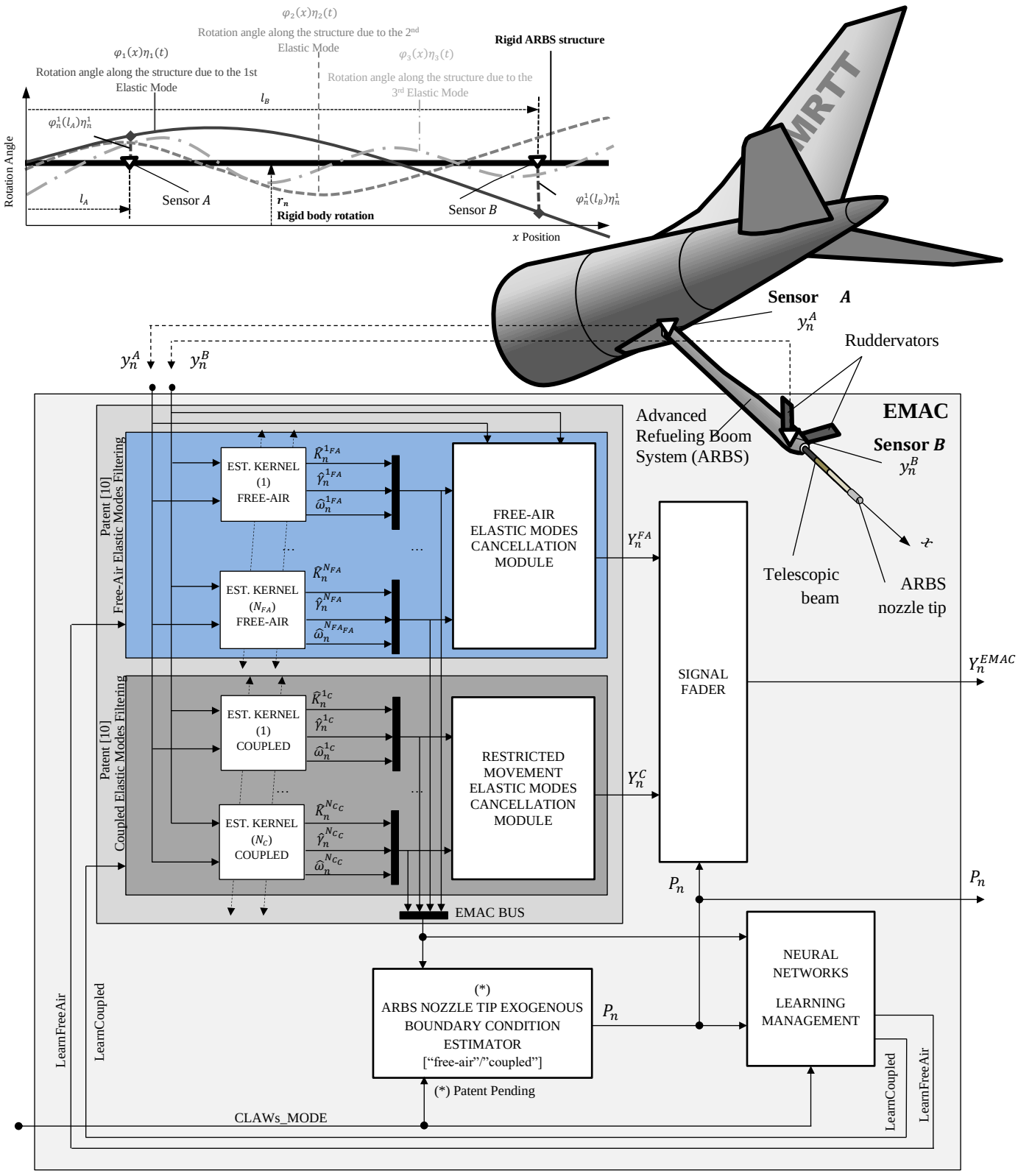

Fig. 1 High-level architecture of the EMAC algorithm

2.1 Elastic Mode Estimation Kernels

Each estimation kernel (depicted in Fig. 2) has been designed to provide the following estimates for a generic i^{th} elastic mode:

1) The estimated $\widehat{K}_n^i$ parameter required to completely cancel the activity of the i^{th} elastic mode by mixing two measurement signals y_n^A and y_n^B measured by sensor A and B.
2) The estimated i^{th} elastic mode activity $\hat{\gamma}_n^i$ in signal y_n^A.
3) The estimated augmented frequency $\hat{\omega}_n^i$ of the i^{th} elastic mode.

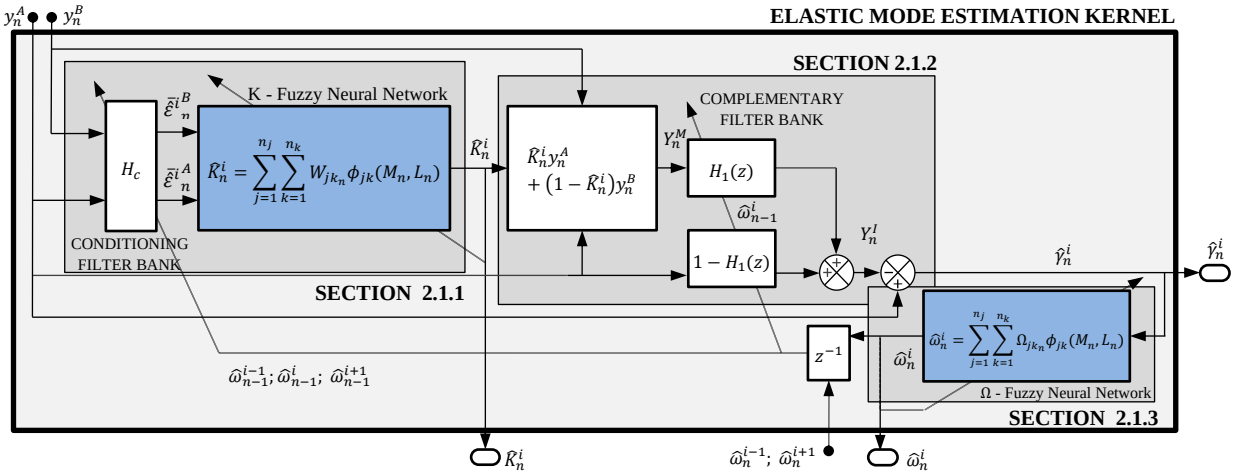

Fig. 2 Block diagram of the elastic mode estimation kernels

2.1.1 Estimating the Elastic Mode Cancellation Parameter K_n^{i*}

The elastic mode cancellation parameters, denoted by K_n^{i*} for a generic i^{th} elastic mode, measure the relative amplitude of the elastic mode component contained in two signals y_n^A and y_n^B. The content of these discrete-time scalar signals can be expressed in terms of the measured rigid and elastic dynamics of the system as follows:

$$y_n^A = r_n + \sum_{j=1}^{N} \varphi_n^j(l_A)\eta_n^j + v_n^A = r_n + \sum_{j=1}^{N} \varepsilon_n^{j\,A} + v_n^A \tag{1}$$

$$y_n^B = r_n + \sum_{j=1}^{N} \varphi_n^j(l_B)\eta_n^j + v_n^B = r_n + \sum_{j=1}^{N} \varepsilon_n^{j\,B} + v_n^B \tag{2}$$

where $l_A \in \mathbb{R}^3$ and $l_B \in \mathbb{R}^3$ denote the spatial location of sensors A and B respectively, $\varphi_n^j(l_A) \in \mathbb{R}$ and $\varphi_n^j(l_B) \in \mathbb{R}$ denote the unitary displacements of the elastic mode j at sensor location l_A and l_B respectively, $\eta_n^j \in \mathbb{R}$ represent the elastic mode generalized coordinate, v_n^A and v_n^B represent the measurement noise in sensor A and B respectively, and r_n is the measured rigid dynamics. The perfect cancellation parameter K_n^{i*} is computed imposing that the linear combination of signals y_n^A and y_n^B results in the perfect suppression of the $\varepsilon_n^{i\,A} = \varphi_n^i(l_A)\eta_n^i$ term in (1), while maintaining unaltered the measured rigid dynamics r_n. Mathematically, this condition can be expressed as:

$$K_n^{i*}\varphi_n^i(l_A)\eta_n^i + \left(1 - K_n^{i*}\right)\varphi_n^i(l_B)\eta_n^i = K_n^{i*}\varepsilon_n^{i\,A} + \left(1 - K_n^i\right)\varepsilon_n^{i*\,B} = 0 \tag{3}$$

Solving (3) for K_n^{i*} yields

$$K_n^{i*} = \frac{\varphi_n^i(l_B)}{\varphi_n^i(l_B) - \varphi_n^i(l_A)} \tag{4}$$

Using equation (4), one can linearly combine signals y_n^A and y_n^B using the K_n^{i*} parameter to perfectly suppress the i^{th} elastic mode component in an output signal Y_n^M as follows:

$$\begin{aligned} Y_n^M &= K_n^{i*} y_n^A + \left(1 - K_n^{i*}\right) y_n^B \\ &= r_n + \sum_{j=1 \neq i}^{N} \left[K_n^{i*} \varphi_n^j(l_A) \eta_n^j + \left(1 - K_n^{i*}\right) \varphi_n^j(l_B) \eta_n^j\right] + K_n^{i*} v_n^A + \left(1 - K_n^{i*}\right) v_n^B \end{aligned} \tag{5}$$

This is a particular case of a spatial filtering technique, where only one elastic mode is cancelled and where any elastic mode different from the i^{th} one is still present in the filtered signal Y_n^M. In a pure model-based design approach, a high-fidelity aeroelastic model could provide information about the unitary displacement functions $\varphi_n^i(l_A)$ and $\varphi_n^i(l_B)$, and thus, K_n^{i*} could be computed using (4). However, by using this approach, any aeroelastic model uncertainty could degrade the elastic mode cancellation performance, leading to a potential reduction of the system stability or even triggering aeroservoelastic coupling instabilities. To prevent this, an adaptive estimator of the K_n^{i*} parameter has been used instead.

For the specific case of the ARBS, it has been proven through aeroelastic simulations and flight test data, that the elastic modes' shapes, and thus the perfect cancellation parameters K_n^{i*}, depend mainly on the telescopic beam length (L_n) and on the Mach number (M_n), and thus, for the ARBS case, $K_n^{i*} = f(L_n, M_n)$. Using the universal approximation theorem, the function $K_n^i = f_i(L_n, M_n)$ can be approximated using an Artificial Neural Network (ANN) as follows:

$$K_n^{i*} = f_i(L_n, M_n) = \widehat{K}_n^i + \sigma = \sum_{j=1}^{n_j} \sum_{k=1}^{n_k} W_{jk_n}^i \phi_{jk}^i(L_n, M_n) + \sigma \tag{6}$$

Where $\widehat{K}_n^i$ is the output of the ANN and denotes the best estimation of the K_n^{i*} parameter (a priori unknown), W_{jk}^i and $\phi_{jk}^i(L, M)$ denote the weights and the activation functions of the ANN for the i^{th} elastic mode, L_n is the n^{th} sample of the telescopic beam length, M_n is the n^{th} sample of the measured Mach number, and σ is a small approximation error. Flight test evidence has shown that the function $f_i(L_n, M_n)$ is smooth in the parameters L and M and thus, a shallow Neural Network with a single layer of activation functions is sufficient to obtain a small approximation error. The selected architecture for the ANN estimator uses triangular activation functions that fulfil the following equations:

$$\sum_{j=1}^{n_j} \sum_{k=1}^{n_k} \phi_{jk}^i(L_n, M_n) = 1 \tag{7}$$

$$\phi_{jk}^i(l_j, m_k) = 1, \qquad \forall j \in [1, n_j], k \in [1, n_k] \tag{8}$$

$$0 \leq \phi_{jk}^i(L_n, M_n) \leq 1, \qquad \forall j \in [1, n_j], k \in [1, n_k] \tag{9}$$

Where l_j and m_k are the breakpoints of a 2D discretization of the ANN's input space $\{L_n \in [L_{MIN}, L_{MAX}],\ M_n \in [M_{MIN}, M_{MAX}]\}$. Every ANN with triangular activations function belongs to the set of Fuzzy Neural Networks (FNN). The main advantage of FNN over other ANN architectures with multi-layer perceptrons is that the weights $W_{jk_n}^i$ of a FNN have a clear physical meaning and interpretability. Moreover, the triangular activation functions in (7-9) provide a simple implementation

of a 2D linear interpolator over a surface, and for each breakpoint L_j and M_k, the following relationship is fulfilled if the FNN has been trained properly:

$$f_i(l_j, m_k) \cong W^i_{jk}, \qquad \forall j \in [1, n_j], k \in [1, n_k] \tag{10}$$

Equation (10) highlights the fact that for any telescopic length $L_n = l_j$ and Mach $M_n = m_k$ (breakpoint coincident), the output of the FNN will be equal the weight $W^i_{jk_n}$, and thus, if the FNN has been trained properly, the weight value and the actual function value $f_i(l_j, m_k)$ will be coincident. For other values of L_n and M_n, there will be still a small approaximation error σ.

From now on, we will refer to the FNNs that estimate the perfect cancellation parameters K^{i*}_n as the K-Fuzzy Neural Networks (K-FNN). Although the K-FNN 's weights $W^i_{jk_n}$ can be computed off-line with a best guess derived from aeroelastic model-based analyses, in order to provide a fully adaptive estimation during the normal operation of the ARBS, the weights $W^i_{jk_n}$ must be modified on-line via a robust update law.

In order to perform this adaptation and training, first, a special conditioning method must be applied to the raw signals y^A_n and y^B_n so as to isolate the i^{th} elastic mode components in both signals, denoted by $\varepsilon^{i\,A}_n$ and $\varepsilon^{i\,B}_n$ in equations (1) and (2). With these components, an estimation error can be computed to update the weights of the K-FNN via backpropagation.

To isolate the i^{th} elastic mode in the signals y^A_n and y^B_n, the estimation kernels use two notch filters (NF) centered at the estimated frequencies $\hat{\omega}^{i-1}_{n-1}$ and $\hat{\omega}^{i+1}_{n-1}$ computed at the previous time step to break the algebraic loop (we will describe their computation in the following subchapter). These notch filters cancel the $i-1$ and $i+1$ elastic modes respectively, and are intended to avoid inter-modal interferences in the estimation of the properties of the i^{th} elastic mode. Posteriorly, both filtered signals are feedforwarded to a band-pass filter (BPF) centered at the estimated frequency of the i^{th} elastic mode computed at the previous time step, denoted by $\hat{\omega}^i_{n-1}$. These steps are represented by the following discrete-time formulas:

$$\begin{aligned}\hat{\varepsilon}^{i\,A}_n &= H_C\left(z^{-1}, \hat{\omega}^{i-1}_{n-1}, \hat{\omega}^{i}_{n-1}, \hat{\omega}^{i+1}_{n-1}\right) \cdot y^A_n \\ &= NF\left(z^{-1}, \hat{\omega}^{i-1}_{n-1}\right) \cdot NF\left(z^{-1}, \hat{\omega}^{i+1}_{n-1}\right) \cdot BPF\left(z^{-1}, \hat{\omega}^{i}_{n-1}\right) \cdot y^A_n\end{aligned} \tag{11}$$

$$\begin{aligned}\hat{\varepsilon}^{i\,B}_n &= H_C\left(z^{-1}, \hat{\omega}^{i-1}_{n-1}, \hat{\omega}^{i}_{n-1}, \hat{\omega}^{i+1}_{n-1}\right) \cdot y^B_n \\ &= NF\left(z^{-1}, \hat{\omega}^{i-1}_{n-1}\right) \cdot NF\left(z^{-1}, \hat{\omega}^{i+1}_{n-1}\right) \cdot BPF\left(z^{-1}, \hat{\omega}^{i}_{n-1}\right) \cdot y^B_n\end{aligned} \tag{12}$$

Where $H_C\left(z^{-1}, \hat{\omega}^{i-1}_{n-1}, \hat{\omega}^{i}_{n-1}, \hat{\omega}^{i+1}_{n-1}\right)$ represent the transfer function of a conditioning filter bank composed of the filters defined in the previous paragraph (see also Fig. 2 for a schematic view of the location of the conditioning filter bank within the elastic mode estimation kernel). Once the estimations of the elastic mode activity have been obtained by the condition filter bank, the signals $\hat{\varepsilon}^{i\,A}_n$ and $\hat{\varepsilon}^{i\,B}_n$ are feedforwarded to a demodulator filter to estimate their amplitudes $\bar{\hat{\varepsilon}}^{i\,A}_n$ and $\bar{\hat{\varepsilon}}^{i\,B}_n$ as follows:

$$\bar{\hat{\varepsilon}}^{i\,A}_n = \frac{1}{2}\sqrt{NF\left(z^{-1}, 2\hat{\omega}^{i}_{n-1}\right) \cdot \left(\hat{\varepsilon}^{i\,A}_n\right)^2} \tag{13}$$

$$\bar{\hat{\varepsilon}}^{i\,B}_n = \frac{1}{2}\sqrt{NF\left(z^{-1}, 2\hat{\omega}^{i}_{n-1}\right) \cdot \left(\hat{\varepsilon}^{i\,B}_n\right)^2} \tag{14}$$

The learning strategy implemented in each one of the estimation kernels is based on a gradient descent technique with backpropagation that tries to minimize a cancellation error E_n^i defined by:

$$E_n^i = \frac{1}{2} {e_n^i}^2 \tag{15}$$

$$e_n^i = \begin{cases} \sum_{j=1}^{n_j} \sum_{k=1}^{n_k} W_{jk_{n-1}}^i \phi_{jk}^i(L_n, M_n) \, {\bar{\varepsilon}_n^i}^A - \left(1 - \sum_{j=1}^{n_j} \sum_{k=1}^{n_k} W_{jk_{n-1}}^i \phi_{jk}^i(L_n, M_n)\right) {\bar{\varepsilon}_n^i}^B & \text{if} \quad K_n^i \text{ is expected to be} \geq 0 \\ \sum_{j=1}^{n_j} \sum_{k=1}^{n_k} W_{jk_{n-1}}^i \phi_{jk}^i(L_n, M_n) \, {\bar{\varepsilon}_n^i}^A + \left(1 - \sum_{j=1}^{n_j} \sum_{k=1}^{n_k} W_{jk_{n-1}}^i \phi_{jk}^i(L_n, M_n)\right) {\bar{\varepsilon}_n^i}^B & \text{if} \quad K_n^i \text{ is expected to be} < 0 \end{cases} \tag{16}$$

$$\min_{W_{jk_n}^i} E_n^i \tag{17}$$

The expected sign of K_n^i, which is required in equation (16), can be obtained from model-based aeroelastic analysis results and flight test data evidence, if any. From now on, for readability purposes, we will consider only those cases where $K_n^i \geq 0$. The K-FNN's weights update law is obtained by differentiation of equation (15) with respect to the weights $W_{jk_n}^i$, yielding:

$$\begin{aligned} W_{jk_n}^i = W_{jk_{n-1}}^i + \Delta W_{jk_n}^i = W_{jk_{n-1}}^i - \lambda_{jk_n} \frac{\partial E_n^i}{\partial W_{jk_n}^i} = W_{jk_{n-1}}^i - \lambda_{jk_n} e_n^i \frac{\partial e_n^i}{\partial W_{jk_n}^i} \\ = W_{jk_{n-1}}^i - \lambda_{jk_n} e_n^i \phi_{jk}^i(L_n, M_n) \left({\bar{\varepsilon}_n^i}^A + {\bar{\varepsilon}_n^i}^B\right) \end{aligned} \tag{18}$$

Where λ_{jk_n} is a learning gain which is dynamically saturated to always grant the numerical stability of the update law [11]. To analyze the numerical stability limits of (18), equation (18) will be expressed as a function of the weight error $\widetilde{W}_{jk_n}^i$ defined as:

$$\widetilde{W}_{jk_n}^i = W_{jk_n}^i - W_{jk}^{i*} \tag{19}$$

Where W_{jk}^{i*} denotes the ideal and unknown weight value that minimizes the cancellation error E_n^i of the i^{th} elastic mode. Using (19), equation (18) can be rewritten as a function of this estimation error to yield:

$$\widetilde{W}_{jk_n}^i = \widetilde{W}_{jk_{n-1}}^i - \lambda_{jk_n} e_n^i \phi_{jk}^i(L_n, M_n) \left({\bar{\varepsilon}_n^i}^A + {\bar{\varepsilon}_n^i}^B\right) \tag{20}$$

Rearranging equation (20) and collecting the terms in $\widetilde{W}_{jk_{n-1}}^i$, as $e_n^i = \sum_{j=1}^{n_j} \sum_{k=1}^{n_k} \widetilde{W}_{jk_{n-1}}^i \phi_{jk}^i(L_n, M_n) \left({\bar{\varepsilon}_n^i}^A + {\bar{\varepsilon}_n^i}^A\right)$, we obtain the following equations:

$$e_n^i = \left(1 - \lambda_{jk_n} \left(\phi_{jk}^i(L_n, M_n) \left({\bar{\varepsilon}_n^i}^A + {\bar{\varepsilon}_n^i}^B\right)\right)^2\right) \widetilde{W}_{jk_{n-1}}^i + \mathrm{o}\left(\widetilde{W}_{lm_{n-1}}^i\right), \ \forall l \neq j, \forall m \neq k \tag{21.1}$$

$$\widetilde{W}_{jk_n}^i = \left(1 - \lambda_{jk_n} \left(\phi_{jk}^i(L_n, M_n) \left({\bar{\varepsilon}_n^i}^A + {\bar{\varepsilon}_n^i}^B\right)\right)^2\right) \widetilde{W}_{jk_{n-1}}^i + \mathrm{o}\left(\widetilde{W}_{lm_{n-1}}^i\right), \ \forall l \neq j, \forall m \neq k \tag{21.2}$$

The first term in right hand side of equation (21.2) is the homogenous part and thus, the numerical stability of the discrete update law will be granted if the following condition holds:

$$\left|1 - \max \lambda_{jk_n} \cdot \left(\phi_{jk}^{i}(L_n, M_n)\left(\bar{\hat{\varepsilon}}_n^{i\,A} + \bar{\hat{\varepsilon}}_n^{i\,B}\right)\right)^2\right| < 1 \tag{22}$$

Rearranging (22) and solving for the maximum value of the learning gain λ_{jk_n} we finally obtain the stability condition for the learning gain λ_{jk_n}:

$$\max \lambda_{jk_n} < \frac{2}{\left(\phi_{jk}^{i}(L_n, M_n)\left(\bar{\hat{\varepsilon}}_n^{i\,A} + \bar{\hat{\varepsilon}}_n^{i\,B}\right)\right)^2} < \lambda_n^{+} \tag{23.1}$$

$$\lambda_n^{+} = \frac{2}{\left(\bar{\hat{\varepsilon}}_n^{i\,A} + \bar{\hat{\varepsilon}}_n^{i\,B}\right)^2} \tag{23.2}$$

The minimum response time of the update law is obtained when $\lambda_{jk_n} = \lambda_n^{*} = 1 \Big/ \left(\bar{\hat{\varepsilon}}_n^{i\,A} + \bar{\hat{\varepsilon}}_n^{i\,B}\right)^2$, and thus, the maximum value of the learning gains λ_{jk_n} is restricted to the value of the minimum time response gain λ_n^{*} with a twosome objective: to grant the numerical stability of the K-FNN's weights update and to avoid the shattering phenomenon in the learning phase that could appear for learning gains $\lambda_n^{*} < \lambda_{jk_n} < \lambda_n^{+}$.

On top of equations (23.1-23.2), a dead zone has been used to avoid the well know parameter drifting problem in the presence of measurement noise [12, 13, 14] as follows:

$$\lambda_{jk_n} = \begin{cases} \min\left(G_i, 1 \Big/ \left(\bar{\hat{\varepsilon}}_n^{i\,A} + \bar{\hat{\varepsilon}}_n^{i\,B}\right)^2\right) & \text{if} \quad e_n^{i}\phi_{jk}^{i}(L_n, M_n)\left(\bar{\hat{\varepsilon}}_n^{i\,A} + \bar{\hat{\varepsilon}}_n^{i\,B}\right) \geq \epsilon_i \\ 0 & \text{if} \quad e_n^{i}\phi_{jk}^{i}(L_n, M_n)\left(\bar{\hat{\varepsilon}}_n^{i\,A} + \bar{\hat{\varepsilon}}_n^{i\,B}\right) < \epsilon_i \end{cases} \tag{24}$$

Where G_i denotes the static learning gain of the estimation kernel of the i^{th} elastic mode, and ϵ_i denotes the threshold of the dead-band. As an additional protection to the learning logic to ensure that the K-FNN's output is always contained within a predefined safety range, the update law in (18) has been adapted to include a real-time weight clipping mechanism as follows:

$$W_{jk_n}^{i} = \min\left(\overline{W}_{jk}^{i}, \max\left(\underline{W}_{jk}^{i}, W_{jk_{n-1}}^{i} - \lambda_{jk_n} e_n^{i}\phi_{jk}^{i}(L_n, M_n)\left(\bar{\hat{\varepsilon}}_n^{i\,A} + \bar{\hat{\varepsilon}}_n^{i\,B}\right)\right)\right) \tag{25}$$

Where $\overline{W}_{jk}^{i}$ and $\underline{W}_{jk}^{i}$ denote a predefined upper and lower bound for the FNN weight $W_{jk_n}^{i}$. These bounds define the confidence space where the K-FNN can learn. A more detailed analysis of the properties of the FNN's weights update law defined in (25) shows that with small elastic activities, the K-FNN weights are kept frozen thanks to the learning dead-zone of (24), but when the elastic activities in the measured signals y_n^{A} and y_n^{B} increase, the cancellation error converges to zero with a rate which is proportional to the square of the sum of the amplitudes of the elastic mode components $\bar{\hat{\varepsilon}}_n^{i\,A}$ and $\bar{\hat{\varepsilon}}_n^{i\,B}$.

2.1.2 Estimating the Elastic Mode Activity γ_n^{i}

With the estimation of the perfect cancellation parameter $\hat{K}_n^{i}$ provided by the K-FNN, each kernel computes an approximation of the i^{th} elastic mode activity in the signal y_n^{A}, denoted with $\hat{\gamma}_n^{i}$ using a second-order parametric band-pass filter $H_1\left(z^{-1}, \hat{\omega}_{n-1}^{i}\right)$ with a notch centered at frequency $\hat{\omega}_{n-1}^{i}$

$$\hat{\gamma}_n^{i} = H_1\left(z^{-1}, \hat{\omega}_{n-1}^{i}\right)\left(1 - \hat{K}_n^{i}\right)\left(y_n^{A} - y_n^{B}\right) \tag{26}$$

2.1.3 Estimating the elastic mode augmented frequency ω_n^i

The last operation performed by the estimation kernels is the estimation of the elastic modes augmented frequencies. We define the augmented frequency, which in general differs from the elastic mode natural frequency, as the frequency of the elastic mode with the flight control laws being in the control loop. Like occurred with the perfect cancellation parameters, the augmented frequencies of the elastic modes mainly depend on the telescopic length and the flight condition. It is customary to obtain an estimation of this function via model-based aeroelastic analyses.

As aeroelastic model uncertainties could degrade the performances of the elastic modes filtering and also the behavior of the boom physical condition estimator (see Section 4.2.3), an adaptive frequency estimator is mandatory. Once again, the methodology of approximating an unknown augmented frequency function $g_i(L_n, M_n)$ via an adaptive Fuzzy Neural Network (named Frequency Fuzzy Neural Network (F-FNN) to differentiate it from the FNN used for the elastic modes perfect cancellation parameters (K-FNN)) has been applied in this case. Flight test evidence again has shown that functions $g_i(L_n, M_n)$ are smooth in the parameters L and M and thus, a single layer Neural Network is sufficient to have a small approximation error for the augmented frequencies. This approximation error can be described as

$$\omega_n^i = g_i(L_n, M_n) = \widehat{\omega}_n^i + \sigma = \sum_{j=1}^{n_j} \sum_{k=1}^{n_k} \Omega_{jk_n}^i \phi_{jk}^i(L_n, M_n) + \delta \tag{27}$$

Where $\widehat{\omega}_n^i$ is the output of the K-FNN, $\Omega_{jk_n}^i$ denotes the weights of the K-FNN for the i^{th} elastic mode, and δ is a small approximation error. In order to minimize the computation time, the activation functions $\phi_{jk}^i(L_n, M_n)$ are shared between the K-FNN and the F-FNN (see equations (7-9)).

In order to achieve the objective of adaptive frequency tracking for each elastic mode, a "slave" notch filter $N_i(z^{-1})$ has been used to provide an indirect estimation of the Neural Network approximation error. The output y_n^i of this "slave" notch filter $N_i(z^{-1})$ will be used to update the K-FNN weights $\Omega_{jk_n}^i$ via backpropagation of the estimation error metric. The term "slave" is intended to highlight the fact that the notch frequency of the filter is linked to the output $\widehat{\omega}_n^i$ of the F-FNN. The key idea is to exploit the frequency information contained in the estimated elastic mode activity signal $\hat{\gamma}_n^i$, defined as

$$\hat{\gamma}_n^i = \hat{\bar{\varepsilon}}_n^i \cos\left(\omega_n^i t_n + \varphi\right) + v_n \tag{28}$$

Where φ is an unknown phase angle, and v_n denotes the set of measurement noise and cross-elastic-mode residuals. As exposed in equation (28), the output y_n^i of a notch filter applied to $\hat{\gamma}_n^i$ will have minimum amplitude if the notch frequency is coincident with the actual elastic mode augmented frequency ω_n^i. Then, if the notch frequency is linked to the F-FNN, the output of the notch filter can be used as a figure of merit of the network approximation error [15].

The schematic architecture of the frequency estimation module implemented in the estimation kernels has been depicted in Fig. 7. The selected "slave" notch filter for this particular case is a parametric second-order IIR filter with a discrete transfer function defined by

$$N_i(z^{-1}; a_n^i, r) = \frac{1 - 2a_n^i z^{-1} + z^{-2}}{1 - 2ra_n^i z^{-1} + r^2 z^{-2}} \tag{29}$$

Where a_n^i is a time-varying parameter defining the notch frequency, r is the pole radius which controls the notch bandwidth ($0 \ll r < 1$). It has to be noted that the transfer function defined in (29) has all the zeros located on the unit circle, and thus, the resulting filter is an infinite-depth IIR notch filter.

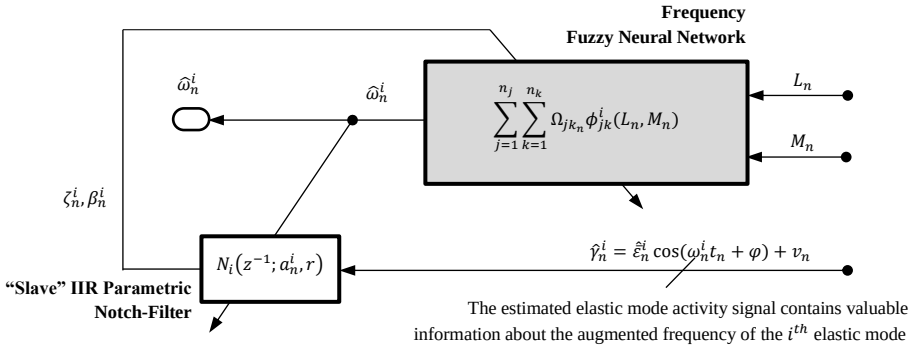

Fig. 3 Schematic view of the frequency estimation module

The "slave" condition is ensured by a unique relationship between the parameter a_n^i and the estimated augmented frequency of the i^{th} elastic mode $\widehat{\omega}_n^i$ provided by the F-FNN. The "slave" equation is defined by

$$a_n^i = \cos\left(\widehat{\omega}_n^i \Delta t\right) = \cos\left(\sum_{j=1}^{n_j}\sum_{k=1}^{n_k}\Omega_{jk_n}^i \phi_{jk}^i(L_n, M_n)\,\Delta t\right) \tag{30}$$

The filter output ζ_n^i can be expressed as follows

$$\zeta_n^i = N_i\left(z^{-1};\widehat{\omega}_n^i\right)\hat{\gamma}_n^i = \hat{\gamma}_n^i - 2a_n^i\hat{\gamma}_{n-1}^i + \hat{\gamma}_{n-2}^i + 2ra_n^i\zeta_{n-1}^i - r^2\zeta_{n-2}^i \tag{31}$$

The objective of the F-FNN training is to minimize a cost function J_n^i defined by the square of the "slave" notch filter output. This cost function is defined by

$$J_n^i = \frac{1}{2}{\zeta_n^i}^2 \tag{32}$$

The cost function value will reach its minimum when the notch-filter output ζ_n^i is close to zero, and thus in this condition of minimum filter output, the estimated augmented frequency $\widehat{\omega}_n^i$ will be equal to the true augmented frequency ω_n^i. The update law of the F-FNN weights $\Omega_{jk_n}^i$ defined in equation (27) is obtained by applying a gradient descent technique to minimize the cost J_n^i as follows

$$\Omega_{jk_n}^i = \Omega_{jk_{n-1}}^i + \Delta\Omega_{jk_n}^i = \Omega_{jk_{n-1}}^i - \mu_{jk_n}\frac{\partial J_n^i}{\partial \Omega_{jk_n}^i} = \Omega_{jk_{n-1}}^i - \mu_{jk_n}\zeta_n^i\frac{\partial \zeta_n^i}{\partial a_n^i}\frac{\partial a_n^i}{\partial \widehat{\omega}_n^i}\frac{\partial \widehat{\omega}_n^i}{\partial \Omega_{jk_n}^i} \tag{33}$$

Where μ_{jk_n} is an adaptive learning gain that grants the numerical stability of the discrete update law in (33). The partial derivative terms in equation (33) can be computed using equations (27), (30) and (31), yielding

$$\frac{\partial \zeta_n^i}{\partial a_n^i} = \beta_n^i = -2\hat{\gamma}_{n-1}^i + 2r\zeta_{n-1}^i + 2ra_n^i\beta_{n-1}^i - r^2\beta_{n-1}^i \tag{34}$$

$$\frac{\partial a_n^i}{\partial \widehat{\omega}_n^i} = \beta_n^i = -\Delta t\sin\left(\widehat{\omega}_n^i\Delta t\right) = -\Delta t\sqrt{1 - {a_n^i}^2} \tag{35}$$

$$\frac{\partial \hat{\omega}_n^i}{\partial \Omega_{jk_n}^i} = \phi_{jk}^i(L_n, M_n) \tag{36}$$

Reordering equation (33), we finally obtain the explicit update law of the F-FNN weights

$$\begin{aligned}\Omega_{jk_n}^i = \Omega_{jk_{n-1}}^i + \mu_{jk_n}\big(&\hat{\gamma}_n^i - 2a_n^i\hat{\gamma}_{n-1}^i + \hat{\gamma}_{n-2}^i + 2ra_n^i\zeta_{n-1}^i \\ &- r^2\zeta_{n-2}^i\big)\beta_n^i\Delta t\sqrt{1-{a_n^i}^2}\,\phi_{jk}^i(L_n, M_n)\end{aligned} \tag{37}$$

$$\beta_n^i = -2\hat{\gamma}_{n-1}^i + 2r\zeta_{n-1}^i + 2ra_n^i\beta_{n-1}^i - r^2\beta_{n-2}^i \tag{38}$$

The adaptive learning gain μ_{jk_n} is computed on-line to grant the numerical stability of (37-38), which holds if

$$\left|1 + \mu_{jk_n}\frac{\left(\left(-2\hat{\gamma}_{n-1}^i + 2r\zeta_{n-1}^i\right)\beta_n^i + \zeta_n^i\delta_n^i\right)\left(1-{a_n^i}^2\right) - \zeta_n^i\beta_n^i a_n^i}{\sqrt{1-{a_n^i}^2}}\Delta t\phi_{jk}^i(L_n, M_n)\right| < 1 \tag{39}$$

$$\mu_{jk_n} < \frac{2\sqrt{1-{a_n^i}^2}}{\Delta t\left|\left(\left(2\hat{\gamma}_{n-1}^i - 2r\zeta_{n-1}^i\right)\beta_n^i + \zeta_n^i\delta_n^i\right)\left(1-{a_n^i}^2\right) + \zeta_n^i\beta_n^i a_n^i\right|} \equiv \mu_n^+ \tag{40}$$

$$\delta_n^i = \frac{\partial \beta_n^i}{\partial a_n^i} = 2r\beta_{n-1}^i - r^2\delta_{n-1}^i \tag{41}$$

Equations (40-41) define the upper stability bound μ_n^+ for the learning gain μ_{jk_n}. Nevertheless, as previously described, the optimal gain for fast adaptation μ_n^* is achieved for $0.5\mu_n^+$ and thus, μ_n^* is selected as the upper bound for the learning gains μ_{jk_n} instead. In order to prevent the parameter drifting phenomenon in the presence of measurement noise, on top of equations (40-41), a dead band has been applied. Thus, the learning gain for each weight of the F-FNN is finally set as:

$$\mu_{jk_n} = \begin{cases}\min\left(G_{\omega_i}, \mu_n^*\right) & \text{if} \quad \Delta\Omega_{jk_n}^i \geq \epsilon_{\omega_i} \\ 0 & \text{if} \quad \Delta\Omega_{jk_n}^i < \epsilon_{\omega_i}\end{cases} \tag{42}$$

Where G_{ω_i} denotes the static learning gain of the estimation kernel of the i^{th} elastic mode, and ϵ_{ω_i} denotes the threshold of the dead-band. As an additional protection to the learning logic, the update law in (37) has been modified to include a real-time weight clipping mechanism to always ensure that the F-FNN output is kept within a predefined safety range

$$\begin{aligned}\Omega_{jk_n}^i = \min\Big(\overline{\Omega}_{jk}^i, \max\big(&\underline{\Omega}_{jk}^i, \Omega_{jk_{n-1}}^i \quad + \\ &\mu_{jk_n}\big(\hat{\gamma}_n^i - 2a_n^i\hat{\gamma}_{n-1}^i + \hat{\gamma}_{n-2}^i + 2ra_n^i\zeta_{n-1}^i - r^2\zeta_{n-2}^i\big)\beta_n^i\Delta t\sqrt{1-{a_n^i}^2}\,\phi_{jk}^i(L_n, M_n)\big)\Big)\end{aligned} \tag{43}$$

Where $\overline{\Omega}_{jk}^i$ and $\underline{\Omega}_{jk}^i$ denote a predefined upper and lower bound for the F-FNN weight $\Omega_{jk_n}^i$. These bounds define the confidence space where the F-FNN can learn.

2.2 The Elastic Modes Cancellation Module

The elastic modes cancellation modules use an extended version of the spatial filtering methodology. The standard spatial filtering methodology uses the information of a sensor array to provide an output signal in which some, or all the elastic modes have been suppressed. In the most general case, the content of a signal y_n^s measured by a sensor s in a sensor array composed by S sensors can be expressed as

$$y_n^s = r_n + \sum_{i=1}^{N} \varphi_n^i(l_s)\eta_n^i + v_n^s \tag{44}$$

And in a more compact form:

$$\boldsymbol{y_n} = r_n\mathbf{1} + \boldsymbol{\Xi\eta_n} + \boldsymbol{v_n} \tag{45}$$

where now $\boldsymbol{y}_n = [y_n^1, \dots, y_n^S]^T \in \mathbb{R}^S, \boldsymbol{v}_n = [v_n^{\mathbf{1}}, \dots, v_n^S] \in \mathbb{R}^S$, $\mathbf{1} \in \mathbb{R}^S$ is a column vector of ones, and $\boldsymbol{\Xi} \in \mathbb{R}^S \times \mathbb{R}^N$ is a matrix containing all elastic modes unitary displacement at sensors locations from $l_1 \in \mathbb{R}^3$ to $l_S \in \mathbb{R}^3$.

$$\boldsymbol{\Xi}_{[S\times N]} = \begin{bmatrix} \varphi_n^1(l_1) & \dots & \varphi_n^N(l_1) \\ \vdots & \ddots & \vdots \\ \varphi_n^1(l_S) & \dots & \varphi_n^N(l_S) \end{bmatrix} \tag{46}$$

Given an a priori known matrix $\boldsymbol{\Xi}$, the spatial filtering algorithm can suppress N elastic modes using a linear combination of the signals y_n^s as follows

$$Y_n^{SF} = \sum_{s=1}^{S} \theta_n^s y_n^s = \boldsymbol{\theta}_n^T\boldsymbol{y_n} = r_n\boldsymbol{\theta}_n^T\mathbf{1} + \boldsymbol{\theta}_n^T\boldsymbol{\Xi\eta_n} + \boldsymbol{\theta}_n^T\boldsymbol{v_n} \tag{47}$$

Where Y_n^{SF} is the output of the spatial filter and $\boldsymbol{\theta}_n = [\theta_n^1, \dots, \theta_n^S]^T \in \mathbb{R}^S$ is a time-varying vector containing the weight coefficients of the spatial filter. In order to keep the measured rigid dynamics unaltered and to perfectly cancel the N elastic modes, the weight coefficients $\boldsymbol{\theta}_n$ shall be compliant with the following equation:

$$\begin{bmatrix} \boldsymbol{\Xi^T} \\ \mathbf{1^T} \end{bmatrix} \boldsymbol{\theta_n} \equiv \boldsymbol{\Phi_n\theta_n} = \begin{bmatrix} \varphi_n^1(l_1) & \dots & \varphi_n^1(l_{N+1}) \\ \vdots & \ddots & \vdots \\ \varphi_n^N(l_1) & \dots & \varphi_n^N(l_{N+1}) \\ 1 & \dots & 1 \end{bmatrix}_{[N+1\times S]} \quad \boldsymbol{\theta_n} = \begin{bmatrix} \mathbf{0_{N\times 1}} \\ 1 \end{bmatrix} \tag{48}$$

Then, solving (48) for weight coefficients vector $\boldsymbol{\theta}_n$ yields

$$\boldsymbol{\theta}_n = \boldsymbol{\Phi^{-1}}[\mathbf{0_{1\times N}} \quad 1]^{\boldsymbol{T}} \tag{49}$$

As can be observed in (49), the standard spatial filtering method requires the matrix $\boldsymbol{\Phi}$ to be invertible in order to cancel the N elastic modes. This mathematical constraint imposes the number of sensors S to be equal to $N + 1$, to make the matrix square. This constraint makes the standard spatial filtering methodology unsuitable for the ARBS. To overcome this intrinsic limitation, an extended spatial adaptive filtering method has been implemented in the elastic modes cancelation modules. This novel method uses the estimated perfect cancellation parameters $\widehat{K}_n^i$ and the estimated elastic mode activities $\hat{\gamma}_n^i$ that have been computed by each one of the elastic modes estimation kernels, to generate a set of $N - 1$ virtual signals, denoted by $\hat{\beta}_n^s$, that complements the already available signals y_n^A and y_n^B. These auxiliary virtual

signals $\hat{\beta}_n^s$ are constructed in such a way that they are linearly independent with respect to their elastic modes contents, so as to be able to generate an invertible matrix $\mathbf{\Phi}$ for the extended spatial filter:

$$\hat{\beta}_n^s = y_n^A - \sum_{i=1}^{N} \xi_n^{i,s} \hat{y}_n^i, \qquad s \in [1, N-1] \tag{50}$$

where $\xi_n^{i,s}$ are parameters that are modified online to grant that the virtual signals are linearly independent with respect to their elastic modes contents. Using the virtual signals $\hat{\beta}_n^s$ as additional measurements provided by a set of $N-1$ virtual sensors, equation (70) can be reformulated for the extended spatial adaptive filter concept, yielding

$$Y_n = \theta_n^1 y_n^A + \theta_n^2 y_n^B + \sum_{j=1}^{N-1} \theta_n^{j+2} \hat{\beta}_n^j \tag{51}$$

Where Y_n is the output of each one of the elastic mode cancellation modules. The new system of equations to be solved in the extended spatial adaptive filtering technique depends on $\xi_n^{i,s}$ parameters, so the elastic modes cancelation module can modify the virtual signals and thus matrix $\hat{\mathbf{\Phi}}_\mathbf{n}$ online as required, granting that it is always proper:

$$\hat{\mathbf{\Phi}}_\mathbf{n} = \begin{bmatrix} 1 & \dots & 1 & 1 \\ \dfrac{\widehat{K}_n^1}{\widehat{K}_n^1 - 1} & \dots & \dfrac{\widehat{K}_n^N}{\widehat{K}_n^N - 1} & 1 \\ \left(1 - \xi_n^{1,1}\right)\dfrac{\widehat{K}_n^1}{\widehat{K}_n^1 - 1} & \dots & \left(1 - \xi_n^{N,1}\right)\dfrac{\widehat{K}_n^N}{\widehat{K}_n^N - 1} & 1 \\ \vdots & \ddots & \vdots & \vdots \\ \left(1 - \xi_n^{1,N-1}\right)\dfrac{\widehat{K}_n^1}{\widehat{K}_n^1 - 1} & \dots & \left(1 - \xi_n^{N,N-1}\right)\dfrac{\widehat{K}_n^N}{\widehat{K}_n^N - 1} & 1 \end{bmatrix}^T \tag{52}$$

Rearranging equations (70) and (73) with (76), the output signal Y_n of each elastic modes cancelation module is computed as:

$$Y_n = \hat{\mathbf{\Phi}}_n^{-1}(\zeta, \widehat{K})[\mathbf{0}_{\mathbf{1}\times\mathbf{N}} \quad 1]^{\boldsymbol{T}}[y_n^A \quad y_n^B \quad \hat{\beta}_n^1 \quad \dots \quad \hat{\beta}_n^{N-1}]^{\boldsymbol{T}} \tag{53}$$

As depicted in Fig. 1, in the current implementation of the EMAC algorithm, there are two independent elastic modes cancellation modules: one dedicated to canceling the first two elastic modes component in "free-air" conditions ($N_{FA} = 2$), which computes the filtered signal Y_n^{FA}, and another one to cancel the first two elastic modes component in "coupled" conditions ($N_C = 2$), which computes the filtered signal Y_n^C as follows:

$$Y_n^{FA} = \hat{\mathbf{\Phi}}_n^{-1}\left(\zeta_{FA}, \widehat{K}_{n_{FA}}^1, \widehat{K}_{n_{FA}}^2\right)[0,0,1]^{\mathrm{T}}\left[y_n^A, y_n^B, \hat{\beta}_{n_{FA}}^1\right]^T \tag{54}$$

$$Y_n^C = \hat{\mathbf{\Phi}}_n^{-1}\left(\zeta_C, \widehat{K}_{n_C}^1, \widehat{K}_{n_C}^2\right)[0,0,1]^{\mathrm{T}}\left[y_n^A, y_n^B, \hat{\beta}_{n_C}^1\right]^T \tag{55}$$

In the previous equations, $\widehat{K}_{n_{FA}}^1$ and $\widehat{K}_{n_{FA}}^2$ denote the estimated perfect cancellation parameter for the first and second elastic mode in "free-air" conditions provided by the "free-air" elastic modes estimation kernels, $\widehat{K}_{n_C}^1$ and $\widehat{K}_{n_C}^2$ denote the estimated perfect cancellation parameter for the first and second elastic

mode in "coupled" conditions provided by the "coupled" elastic modes estimation kernels, and $\hat{\beta}^1_{n_{FA}}$ and $\hat{\beta}^1_{n_C}$ denote the virtual signals generated for "free-air" and "coupled" conditions respectively.

2.3 Physical Status Estimator and Signal Fader

The exogenous physical boundary conditions acting on the ARBS' nozzle may limit the displacements of the flexible structure and can impose certain restrictions on the degrees of freedom of the system, which ultimately modify its aeroservoelastic properties. Fast discrete changes in these exogenous physical boundary conditions need to be identified rapidly in order to select the proper filtered signal (Y_n^{FA} or Y_n^C) to feed the BCLAWs' controllers, with independency of the automatic control mode transition functionality and the CLAWs control mode being active.

To fulfil this objective, a physical status estimator has been implemented in the EMAC algorithm to compute the estimated probability for the ARBS of being actually in restricted movement conditions. This estimator uses the data provided by the elastic modes estimation kernels to monitor the elastic energy around two frequency bandwidths associated with the first elastic mode in free-air and restricted-movement status. Depending on the energy content in these frequency bandwidths and the BCLAWs' control mode being active, the algorithm is capable of computing the probability P_n for the ARBS of being in restricted movement conditions.

The probability P_n computed by the physical status estimator is used to construct the EMAC's algorithm output signal Y_n^{EMAC} as the weighted sum between the "free-air" and the "coupled" filtered signals as follows:

$$Y_n^{EMAC} = P_n Y_n^C + (1 - P_n) Y_n^{FA} \tag{56}$$

2.4 Fuzzy Neural Networks Online Training Management

As illustrated in Fig. 1, the elastic modes estimation kernels are divided in two different sets, those dedicated to analyse the properties of the elastic modes in "free-air" conditions, and those dedicated to analyse the elastic modes properties in "coupled" conditions. The FNN of the "free-air" elastic mode estimations kernels shall be trained only when there is high confidence of the ARBS for being in "free-air" conditions, with independency of the CLAWs control modes being active. On the other hand, the FNN of the "coupled" elastic modes estimation kernels shall be trained only when there is high confidence of the ARBS being in "coupled" conditions. To accomplish this requirement, EMAC algorithm also uses the estimated probability of being in restricted-movement conditions P_n to determine when and what FNN is going to be trained online.

3 Flight Test Results

With the aim to validate the robustness and performance of the EMAC algorithm, a dedicated flight test campaign was performed during the winter of 2019 over the Alboran Sea with an A310 MRTT testbed and during the autumn of 2020 with the new A330 SMART MRTT. In this section we will show some of the results obtained during the campaign, illustrating two specific functionalities of the EMAC algorithm, the adaptive aeroservoelastic coupling suppression functionality, and the real-time estimation of the exogenous boundary condition acting on the ARBS nozzle tip with a simulated coil signal failure during operational contacts with a squadron of Lockheed Martin F-16A from the Portuguese Air Force acting as the receiver aircraft.

For this test, ad-hoc modifications in the Boom Control Unit software were required to simulate the failure to receive the coil-pulse generated by the F-16A receptacle in order to reproduce undetected Control Mode Mismatch failure conditions in a controlled environment. One of the main objectives of this test was to check the capability of the EMAC algorithm to detect the "contact" with the F-16A using information only from the measurement sources A and B in a failure condition.

In the flight envelope point where the test was performed, without the EMAC algorithm, the advent of an aeroservoelastic coupling phenomenon triggering an unstable motion in the lateral axis of the ARBS after the "contact" was expected if the BCLAWs control mode was kept in "free-air" mode. Time histories of y_n^A and Y_n^{EMAC} signals representing the measured and filtered ARBS roll angle respectively have been depicted in the upper subplot of Fig. 4 (a legacy non-adaptive filter was applied to the attitude feedback signal in this test, and the signal Y_n^{EMAC} provided by the EMAC algorithm was used only for monitoring purposes). The BCLAWs control mode and the estimated probability of being in "restricted-movement" conditions (P_n), computed by EMAC algorithm, has been represented in the middle subplot. Finally, the measured lateral force in the ARBS nozzle tip has been shown in the bottom subplot in order to better visualize the lateral aeroservoelastic coupling instability phenomenon generated by the Control Mode Mismatch failure case (see the increasing lateral force amplitude after Time = 8sec in Fig. 4). The test

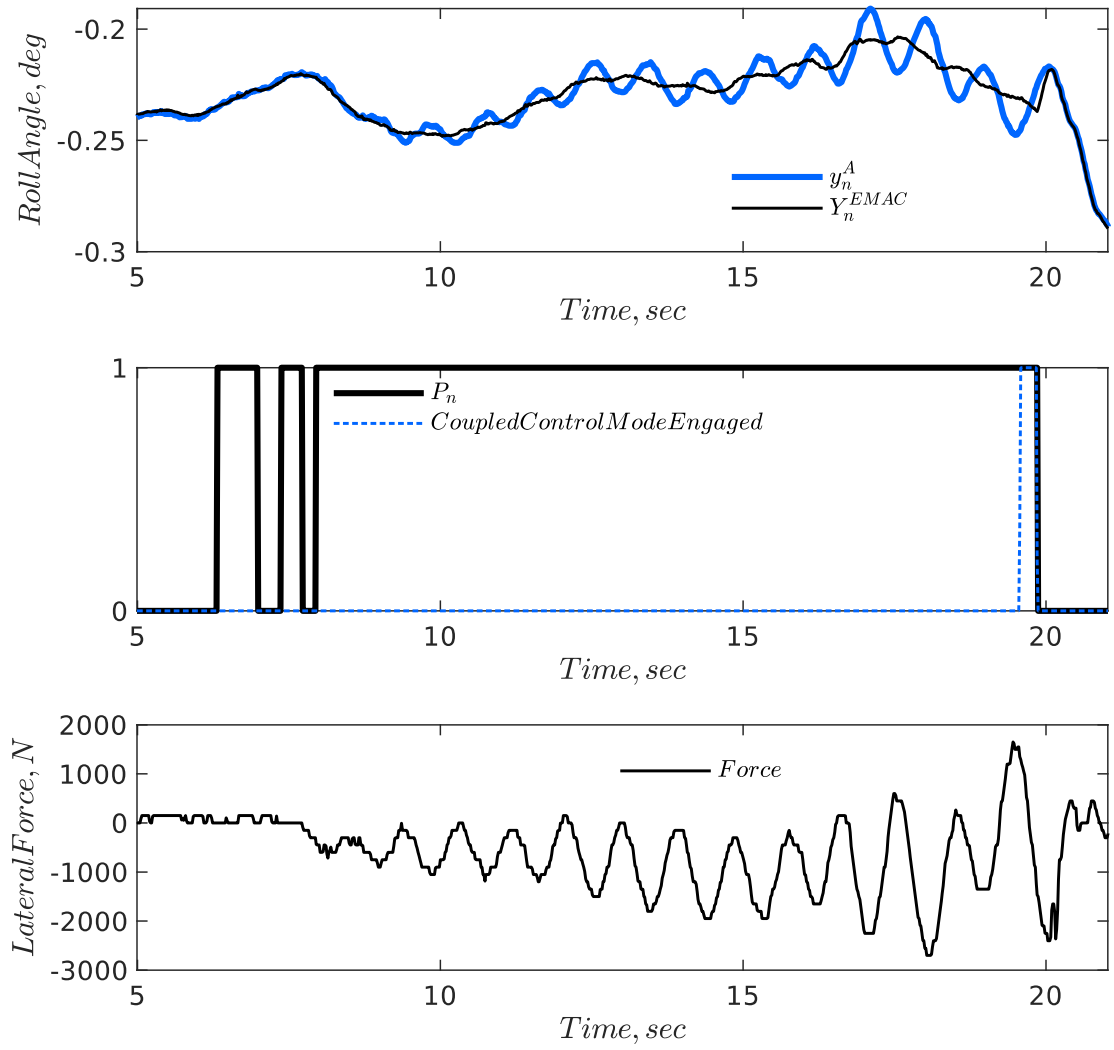

Fig. 4 Undetected Contact flight test results with the EMAC algorithm disabled. Observe the aeroservoelastic coupling instability onset when the flying boom is in Control Mode Mismatch in this non-operational flight condition (BCLAWs in Free-Air control mode while the boom is actually latched to the

with the EMAC filtering disabled was conducted safely with maximum lateral forces of 2500N, and the expected unstable aeroservoelastic coupling phenomenon was reproduced satisfactorily.

A second test was performed in the same flight conditions of the previous example, but this time with the EMAC adaptive filtering and the exogenous boundary condition estimator enabled. The test results have been shown in Fig. 5, where it can be clearly observed that the EMAC algorithm was able to detect the "contact" condition (defined by those instants where $P_n > 0.9$). Note that the measured nozzle force signal is not used by the EMAC algorithm to estimate the exogenous boundary conditions acting on the ARBS nozzle tip (the algorithm can be used also in case of a failed force signal). Moreover, thanks to the adaptive filtering of the EMAC algorithm, the aeroservoelastic coupling phenomenon was suppressed (note that the damping of the oscillations observed in the measured lateral force signal shown in the bottom subplot of Fig. 5 is related to the natural structural and aerodynamic damping of the first elastic mode in "coupled" conditions).

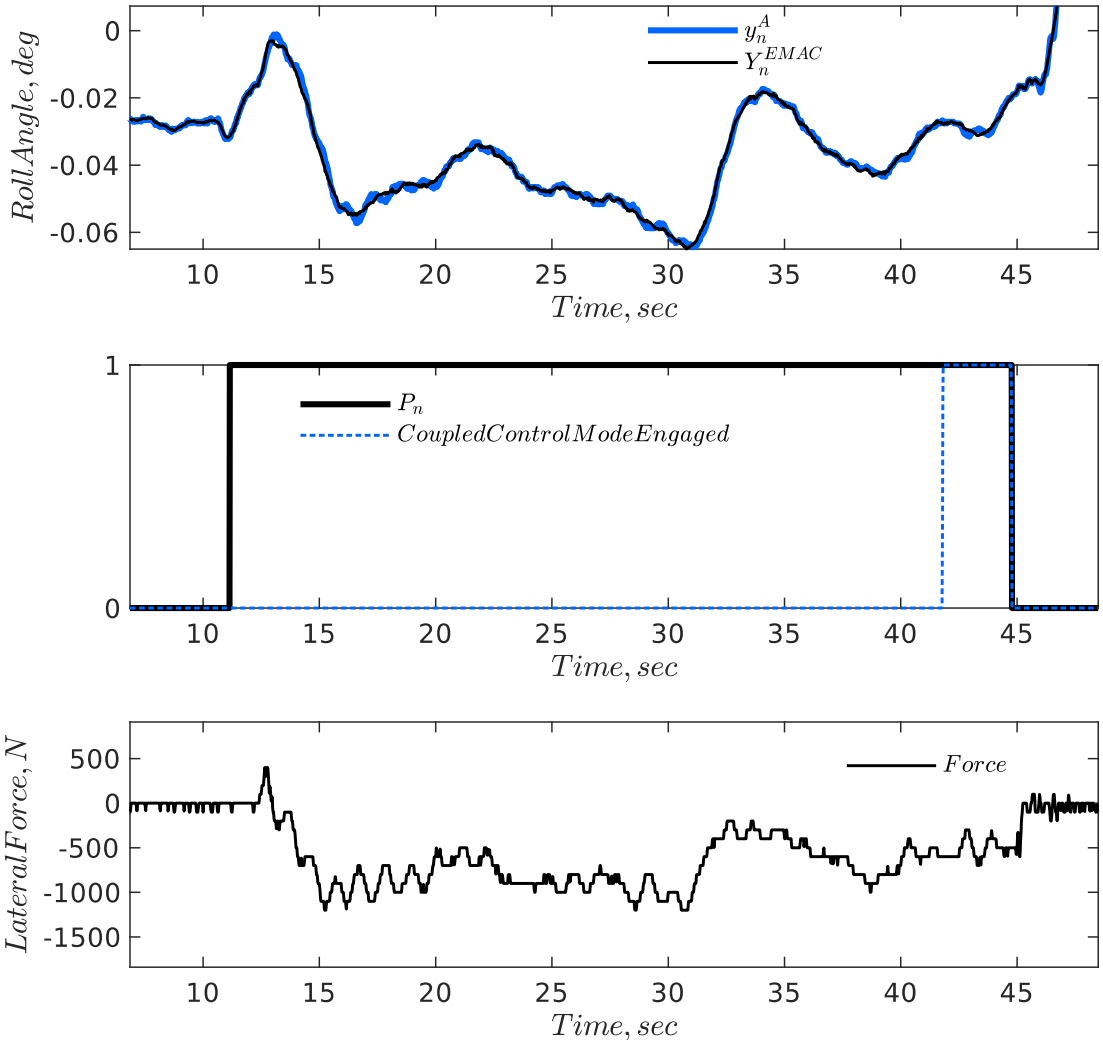

Fig. 5 Undetected Contact flight test results, with the EMAC algorithm enabled. Observe the absence of aeroservoelastic coupling.

4 Conclusions

The Elastic Modes Adaptive Cancellation method was created to solve the constraints of existing filtering algorithms in isolating the flexible dynamic in a feedback signal of a controlled system, with zero phase loss and attenuation. This algorithm has proven to be capable of cancelling all selected elastic modes, with a very limited number of sensors (only two are required) and with limited previous knowledge of the elastic characteristics of the system, using adaptive estimation kernels that identify their properties in real-time.

The EMAC algorithm has been successfully validated through several flight test campaigns since 2017, with the A310 MRTT flight testbed and the A330 SMART MRTT, demonstrating that it provides the BCLAWs with an increased robustness level to unmodelled elastic dynamics and undetected failures, including Control Mode Mismatch conditions, then, increasing the safety level of Air to Air Refueling operations with the ARBS.

Future work includes the development of adaptive modal augmentation and adaptive flutter control functionalities using the elastic mode activity provided by the EMAC algorithm.

References

[1] Pratt, R., Flight Control Systems: Practical Issues in Design and Implementation, Institution of Electrical Engineers, 2010.

[2] Felt, L. R., Huttsell, L. W., Noll, T. E., and Cooley, D. E., "Aeroservoelastic Encounters," Journal of Aircraft, Vol. 16, No. 7, 1979, pp. 477–483.

[3] Luber, W. en Becker, J. (05 2000) "An Integrated Design Procedure for Aircraft Structure Including the Influence of Flight Control System on Aircraft Flutter", bl 15.

[4] Vatankhah, R., Karami, F. en Salarieh, H. (2015) "Observer-based vibration control of non-classical microcantilevers using extended Kalman filters", Applied Mathematical Modelling, 39(19), bll 5986–5996. doi: 10.1016/j.apm.2015.01.047.

[5] Meirovitch, L. en Baruh, H. (1985) "The implementation of modal filters for control of structures", Journal of Guidance, Control, and Dynamics, 8(6), bll 707–716. doi: 10.2514/3.20045.

[6] Pusch, M., Ossmann, D. και Luspay, T. (2019) 'Structured Control Design for a Highly Flexible Flutter Demonstrator', Aerospace, 6(3). doi: 10.3390/aerospace6030027.

[7] Britt, R. T., Volk, J. A., Dreim, D. R., & Applewhite, K. A. (1999). "Aeroservoelastic Characteristics of the B-2 Bomber and Implications for Future Large Aircraft."

[8] Shelley, S.J. , 1991, "Investigation of discrete modal filters for structural dynamic applications," Ph.D. thesis, University of Cincinnati, OH.

[9] Bosse, A., Lim, T. W. en Shelley, S. (2000) "Modal Filters and Neural Networks for Adaptive Vibration Control", Journal of Vibration and Control, 6(4), bll 631–648. doi: 10.1177/107754630000600408.

[10] Rodríguez Robles, R., Asensio Nieto, F., and Sanz de Blas, A., Airbus Defence and Space, Getafe, Madrid, Spain. Patent Application for a "Method for Adaptively Cancelling in Real Time Elastic Modes in Discrete-Time Signals". Patent Publication No. EP 3299790 A1 and US 2018088000 A1, filed 25 Sept. 2017.

[11] ‘5.7 Linear Stability Analysis of Discrete-Time Nonlinear Dynamical Systems’ (2020). Binghamton University, State University of New York.

[12] Lawrence, D. A., Sethares, W. A. en Ren, W. (1990) “Parameter drift instability in adaptive systems”, in 29th IEEE Conference on Decision and Control, bll 3230–3235 vol6. doi: 10.1109/CDC.1990.203388.

[13] C. Wilkinson, J. L., Bharadwaj, R., and Woodham, K., “Verification of Adaptive Systems”. FAA Technical Report DOT/FAA/TC-16/4. April 2016.

[14] Bhattacharyya, S., Cofer, D., Musliner, D. J., Mueller, J. and Engstrom, E., “Certification Considerations for Adaptive Systems”. NASA Technical Report NASA/CR–2015-218702., March 2015.

[15] Kinugasa, Y., Itoh, Y., Kobayashi, M., Fukui, Y. and Okello, J., “A study on the step size of cascaded adaptive notch filter utilizing allpass filter”. IEEJ Transactions on Electronics, Information and Systems. 123. IV-401. 10.1109/ISCAS.2003.1205859.